PHYSICAL REVIEW A VOLUME 36, NUMBER 4 AUGUST 15, 1987

Correlation effects in elastic e-N_2 scattering

Winifred M. Huo*
Radiation Laboratory, University of Notre Dame, Notre Dame, Indiana 46556

Marco A. P. Lima,† Thomas L. Gibson,‡ and Vincent McKoy
Arthur Amos Noyes Laboratory of Chemical Physics, California Institute of Technology, Pasadena, California 91125
(Received 24 February 1987)

The Schwinger multichannel formulation has been applied to study the role of electron correlation in low-energy e-N_2 scattering. For the five nonresonant partial-wave channels studied here, $^2\Sigma_g^+$, $^2\Sigma_u^+$, $^2\Pi_u$, $^2\Delta_g$, and $^2\Delta_u$, we find angular correlation to be much more important than radial correlation. Our results for the $^2\Sigma_g^+$ channel are in agreement with those of Schneider and Collins [Phys. Rev. A **30**, 95 (1984)]. Our calculated total and differential cross sections agree with experiment except for the differential cross sections at 1.5 eV. Our results are also compared with those obtained using model polarization potentials.

I. INTRODUCTION

Correlation or polarization effects play an important role in low-energy electron-molecule collisions. A number of theoretical methods have been developed for describing these effects, including the use of polarization potentials with an empirical cutoff function.[1] Onda and Temkin[2] and Gibson and Morrison,[3] among others, have employed the polarized orbital method[4] to construct *ab initio* polarization potentials. Padial and Norcross[5] introduced a correlation-polarization potential where the short-range correlation effects are approximated by the electron-gas model. In close-coupling expansions, correlation is described by virtual excitations to energetically inaccessible electronic states of the target, i.e., closed channels. This approach is also used in the R-matrix method,[6] where correlation is introduced through the inclusion of pseudostates inside the R-matrix region.[7] Similarly, the Schwinger multichannel method (SMC)[8–11] treats correlation by explicitly including closed-channel functions in the expansion of the $(N+1)$-electron wave function. On the other hand, the optical potential approach[12–16] incorporates the effect of virtual excitations to target excited states in a nonlocal, energy-dependent optical potential for the continuum electron.

Generally, correlation can be grouped into two different types: radial correlation (or in-out correlation) where the closed-channel target state is of the same symmetry as the initial state, and angular correlation where the initial and closed-channel states are of different symmetry. In particular, if the closed-channel target state is coupled to the initial state by a dipole-allowed excitation, the angular correlation term reduces to the standard polarization potential at large electron-target separation. In a recent paper, Schneider and Collins[15] applied the optical potential method to study correlation effects in the $^2\Sigma_g^+$ and $^2\Pi_g$ channels in low-energy e-N_2 scattering. They found different types of correlation to be important in these two channels. Based on the relation of angular correlations to the long-range polarization potential, they used the terms short-range polarization for radial correlation and long-range polarization for angular correlation. We choose to use the terms radial and angular correlations to conform with the standard terminology in quantum chemistry. We also use the term correlation instead of polarization to describe these effects. Polarization provides an appropriate description in a two-step polarization potential calculation where the distortion of the bound electrons by the free electron is considered first and then the distorted molecular charge distribution is used to generate a potential for the continuum electron. In the SMC method, the mutual distortion of the free and bound electrons is treated simultaneously, instead of stepwise, by the closed-channel configurations in the wave function and correlation is a more suitable term in this case.

In the preceding paper,[11] hereafter referred to as I, we present the results of a study on the $^2\Pi_g$ channel in e-N_2 elastic scattering. Consistent with the results of Schneider and Collins,[15] we found that radial correlation is dominant for this channel. Inclusion of angular correlation lowers the resonance position well below experiment, indicating a differential correlation effect among bound electrons in the N_2 and $e+N_2$ systems. In this paper, we study correlation effects in the other partial-wave channels important in low-energy e-N_2 scattering. The present calculation, together with the results from I, provides us with a set of elastic scattering cross sections and momentum transfer cross sections which can be used in the modeling of reentry flow fields, swarm experiments, and plasma etching experiments. The momentum transfer cross sections, for this and other systems, will be reported elsewhere.[17]

The SMC formulation has been reviewed in paper I and will not be repeated here. Section II gives the computational details and our results are presented in Sec. III.

II. COMPUTATIONAL PROCEDURES

A SMC calculation involves the determination of the following quantities: (a) a Gaussian basis to expand the

$(N+1)$-electron wave function, $\Psi_0^{(+)}$, (b) an insertion basis for the separable representation of the free-particle Green's function, (c) a set of molecular orbitals in terms of basis (a), to be used in forming the Slater determinants in the expansion of $\Psi_0^{(+)}$, and (d) the closed-channel configurations to describe correlation. Once these four quantities are chosen, the scattering amplitude is determined by the fractional form of the multichannel Schwinger variational principle.[8-11]

The present calculation used Gaussian basis set B described in paper I. We chose this basis set because the calculated polarizability and quadrupole moment are in good agreement with experiment. The basis set is well balanced, and not biased toward a particular partial-wave channel.

Five different insertion basis sets are used in the representation of the free-particle Green's function, depending on the symmetry of the partial wave. All five insertion bases include the original Gaussian basis set for $\Psi_0^{(+)}$, and supplementary functions are added for all partial-wave channels except the $^2\Delta_u$. They are shown in Table I. As described in paper I, we checked the quality of the insertion bases by calculating the unitarity of the S matrix using the α-insertion technique (see Ref. 11) and we found approximately a 3% deviation from unitarity using the insertion basis sets presented here.

The choice of molecular orbitals and closed-shell configurations is important because we use a limited set of closed-channel configurations for $\Psi_0^{(+)}$:

$$\Psi_0^{(+)} = \sum_k c_k \mathcal{A}(\phi_1\phi_2\cdots\phi_n\phi_k) + \sum_{i,j,k} c_{ij,k} a_j a_i^\dagger \mathcal{A}(\phi_1\phi_2\cdots\phi_n\phi_k) \,. \quad (1)$$

Here $\mathcal{A}$ is an antisymmetrization operator. The first term in Eq. (1) gives the static exchange contribution, with $\phi_1, \phi_2, \ldots, \phi_n$ the target self-consistent-field (SCF) orbitals, and the set of ϕ_k's orthogonalized to the target orbitals. In our calculation, the *full* set of ϕ_k generated from the Gaussian basis is always used for this term. Thus, the result is independent of the choice of orbitals. The second term gives the closed-channel configurations which describe the mutual distortion of the incoming electron and the target. Since we only used a selected set of closed-channel configurations, the quality of the calculation depends on a judicious choice of molecular orbitals and closed-channel configurations. The molecular orbitals used in the present calculation belong to the same set of natural orbitals used in I. They were determined from a bound-state polarization configuration-interaction[18] (POLCI) calculation of the $^2\Sigma_g^+$ state of N_2^-. As discussed in I, such a bound-state calculation does not provide a proper description of the continuum electron. Nevertheless, a truncated set of natural orbitals, selected according to their occupation numbers, appears to describe the relaxation of the target in the presence of the extra electron very efficiently. In using the same set of natural orbitals from a $^2\Sigma_g^+$ CI calculation in the other partial-wave channels, we assume that the correlating orbitals describing molecular relaxation are relatively insensitive to the symmetry of the continuum electron. We tested this idea first on the $^2\Pi_g$ channel and found very little difference in the cross sections using natural orbitals calculated with different symmetries. Thus, the $^2\Sigma_g^+$ natural orbitals were used in the calculations of all partial-wave channels.

Considerable effort was required to determine an optimal set of closed channel configurations. Table II presents the hole (ϕ_i), particle (ϕ_j), and scattering (ϕ_k) orbitals used to represent the closed channels in the $^2\Sigma_g^+$ calculation. The closed-channel configurations for the other partial waves can be generated by suitable replacement of the scattering orbitals. In the five partial-wave channels studied here, angular correlation is more important than radial. Thus, the physical picture in correlating these partial-wave channels is the reverse of the case for the $^2\Pi_g$ channel reported in paper I. To illustrate the effect of various correlation terms, Table III shows the $^2\Sigma_g^+$, $^2\Sigma_u^+$, and $^2\Pi_u$ cross sections at selected incident energies and calculated using angular correlation alone, radial correlation alone, and angular and radial correlations combined. The closed-channel configurations used in these calculations are given in Table II (with suitable change of scattering orbitals for $^2\Sigma_u^+$ and $^2\Pi_u$ symmetries) except for the calculation using radial correlation only. In that case we expanded the hole space to include the $2\sigma_g$ and $2\sigma_u$ orbitals. The particle and scattering space

TABLE I. Gaussian basis sets used in the representation of $G_P^{(+)}$.

Basis set	Exponent
$^2\Sigma_g^+$ channel: Basis set for $\Psi_0^{(+)}$ plus 15 s functions at midpoint	4800, 2400, 1200, 600, 480, 240, 120, 60, 30, 15, 8, 4, 2, 1, 0.25
$^2\Sigma_u^+$ channel: Basis set for $\Psi_0^{(+)}$ plus 15 p_z functions at midpoint	4800, 1200, 600, 300, 120, 60, 30, 15, 8, 4, 2, 1, 0.25, 0.01, 0.001
$^2\Pi_u$ channel: Basis set for $\Psi_0^{(+)}$ plus 15 p_x functions at midpoint	4800, 1200, 600, 300, 120, 60, 30, 15, 8, 4, 2, 1, 0.25, 0.01, 0.001
$^2\Delta_g$ channel: Basis set for $\Psi_0^{(+)}$ plus 10 d_{xy} functions at midpoint plus 5 d_{x^2} and 5 d_{y^2} functions at midpoint	d_{xy}: 4800, 1200, 480, 120, 30, 8, 2, 0.25, 0.01, 0.001 d_{x^2}, d_{y^2}: 4800, 480, 48, 4.0, 0.25
$^2\Delta_u$ channel: Basis set for $\Psi_0^{(+)}$	

TABLE II. Closed-channel configurations used for the $^2\Sigma_g^+$ channel.

ϕ_i	ϕ_j	ϕ_k
Angular correlation		
$3\sigma_g$	3, 4, $5\sigma_u$	3, 4, $5\sigma_u$
	2, 3, $4\pi_{ux}$	2, 3, $4\pi_{ux}$
	2, 3, $4\pi_{uy}$	2, 3, $4\pi_{uy}$
$1\pi_{ux}$	4, 5, 6, $7\sigma_g$, 1, $2\delta_{g(x^2-y^2)}$	2, 3, 4, $5\pi_{gx}$
	1, 2, $3\pi_{gx}$	3, $4\sigma_u$, 1, $2\delta_{u(x^2-y^2)}$
	1, 2, $3\delta_{gxy}$	2, 3, $4\pi_{uy}$
$1\pi_{uy}$	4, 5, 6, $7\sigma_g$, 1, $2\delta_{g(x^2-y^2)}$	2, 3, 4, $5\pi_{gy}$
	1, 2, $3\pi_{gy}$	3, $4\sigma_u$, 1, $2\delta_{u(x^2-y^2)}$
	1, 2, $3\delta_{gxy}$	2, 3, $4\pi_{ux}$
$2\sigma_u$	4, 5, 6, $7\sigma_g$	3, 4, $5\sigma_u$
	1, 2, $3\pi_{gx}$	2, 3, $4\pi_{ux}$
	1, 2, $3\pi_{gy}$	2, 3, $4\pi_{uy}$
$2\sigma_g$	3, $4\sigma_u$	3, 4, $5\sigma_u$
	2, $3\pi_{ux}$	2, 3, $4\pi_{ux}$
	2, $3\pi_{uy}$	2, 3, $4\pi_{uy}$
Radial correlation		
$3\sigma_g$	5, $6\sigma_g$	4, 5, $6\sigma_g$
$1\pi_{ux}$	2, $3\pi_{ux}$	4, 5, $6\sigma_g$
$1\pi_{uy}$	2, $3\pi_{uy}$	4, 5, $6\sigma_g$

were also expanded. All calculations were carried out at $R=2.068$ a.u.

Schneider and Collins[15] have reported a similar study of correlation effects in the $^2\Sigma_g^+$ partial-wave channel using the linear-algebraic-optical-potential method. Their cross sections are also presented in Table III. A comparison with their results shows that the difference between the cross sections obtained using angular correlation alone and combined angular and radial correlations is smaller in our case. Otherwise, the two sets of calculations are similar. The numerical differences between the two are probably due to differences in basis sets and the choice of the closed-channel space. Using a semiempirical polarization potential with the cutoff parameter chosen to fit the experimentally observed position of the $^2\Pi_g$ resonance, Morrison and Collins[19] obtained a value of 41.674 a.u. at 0.05 a.u., significantly larger than the present result of 30.89 a.u. and the value of 26.89 a.u. from Schneider and Collins. The recent calculation of Gibson *et al.*[20] reported a value of 34.387 a.u. obtained with an *ab initio* polarization potential deduced using the polarized orbital method. Their result reflects a better treatment of short-range angular correlations. The remaining difference between their result and the present *ab initio* value may be due to their use of a nonpenetrating approximation.[4]

The polarization potential of Padial and Norcross[5] differs from the two discussed above in their use of the

TABLE III. Comparison of angular and radial correlation effects in the $^2\Sigma_g^+$, $^2\Sigma_u^+$, and $^2\Pi_u$ channels.[a]

	Present result (a.u.)	Schneider and Collins[b] (a.u.)
$^2\Sigma_g^+$ cross section at 0.1 Ry		
Angular correlation only	31.35	29.59
Radial correlation only	48.64	49.49
Angular + radial correlations	30.89	26.80
$^2\Sigma_u^+$ cross section at 0.2 Ry		
Angular correlation only	2.25	
Radial correlation only	4.83	
Angular + radial correlations	2.18	
$^2\Pi_u^+$ cross section at 0.2 Ry		
Angular correlation only	0.41	
Radial correlation only	2.69	
Angular + radial correlations	0.35	

[a]Calculated at $R=2.068$ bohr.
[b]Reference 14.

electron-gas model to describe short-range correlation. A comparison with their cross sections reveals some interesting features of that potential. Our $^2\Sigma_g^+$ cross section appears to agree well with their data using ESECOP (exact static-exchange correlation polarization), an indication that the short-range angular correlation is probably treated correctly in their potential. On the other hand, they reported a position (2.17 eV) and width (0.47 eV) for the $^2\Pi_g$ resonance, which are in much better agreement with our calculation excluding angular correlation (2.29 and 0.41 eV, respectively). This discrepancy in their description of correlation effects may well be due to their use of the electron-gas approximation.

The present calculations support the conclusion drawn by Schneider and Collins[15] that the lack of δ functions in the basis set of Burke, Noble, and Salvini[22] is the source of the large $^2\Sigma_g^+$ cross sections from their R-matrix calculations. While the R-matrix method should, in principle, provide the same type of *ab initio* treatment of electron correlation as presented here, their $^2\Sigma_g^+$ cross section, 55.78 a.u., is significantly larger than the *ab initio* values in Table III. The importance of δ functions is illustrated in a calculation using Gaussian basis set A of paper I, i.e., without the $\delta_{x^2-y^2}$ functions but keeping one of the δ_{xy} functions. This calculation gave a value of 39.79 a.u. for the $^2\Sigma_g^+$ cross section, significantly larger than the value of 30.89 a.u. when $\delta_{x^2-y^2}$ functions are included. In view of this result, it should not be surprising that the $^2\Sigma_g^+$ cross section of Burke *et al.* is significantly larger than other *ab initio* values.

For the $^2\Pi_g$ channel, we found a significant differential correlation effect. The same question may be raised for the five partial-wave channels studied here. Is a POLCI treatment of correlation, which neglects the differential correlation effect between the bound electrons in N_2 and $e+N_2$, sufficient to provide reliable cross sections for these channels? A comparison between the calculated cross sections with experiment in Sec. III indicates that the differential correlation effect is probably small in these channels.

III. RESULTS AND DISCUSSIONS

The integral cross section for the $^2\Sigma_g^+$, $^2\Sigma_u^+$, $^2\Pi_u$, $^2\Delta_g$, and $^2\Delta_u$ partial-wave channels are tabulated in Table IV. All calculations include both angular and radial correlations and were carried out at $R=2.068$ a.u. Static-exchange calculations at other R values showed a very weak R dependence in these cross sections, at least at this level of approximation. For example, the $^2\Sigma_g^+$ static-exchange cross section decreases by 8% as R increases from 1.7 to 2.3 a.u. In view of this result, the fixed nuclei cross sections for the five partial-wave channels reported here should be directly comparable with experiment. The same situation holds for the nonresonant contributions in the $^2\Pi_g$ channel. On the other hand, an appropriate treatment of the nuclear dynamics is required for the resonant $l=2$, $m=1$ partial wave in that channel. This was done by first deducing the width and shift functions from the electronic calculation reported in paper I and then doing the nuclear dynamics calculation with the Feshbach projection operator formalism. The procedure we used has been described previously.[21] Theoretical total cross sections are determined using this hybrid form of fixed-nuclei cross sections for the nonresonant channels and nuclear dynamics calculations for the resonant channels from $v=0$ to $v=0$–8. Figure 1 compares the theoretical total cross-section curve with the experimental data of Kennerly,[22] Hoffman *et al.*,[23] and Baldwin.[24] In the nonresonant region, the theoretical cross sections are about 10% lower than Kennerly's experiment. The deviation from the other two sets of data is slightly larger. The discrepancy may be due to limitation of the basis set, the use of a noniterative procedure in the solution of the SMC equations, neglect of correlation among the bound electrons, and the use of the fixed-nuclei approximation in the nonresonant channels. In view of these considerations, the agreement is reasonable. In the resonant region, the present calculation gives the correct peak positions but the calculated peak heights are somewhat higher than experiment for the first three peaks and become lower

TABLE IV. Integral cross sections for the $^2\Sigma_g^+$, $^2\Sigma_u^+$, $^2\Pi_u$, $^2\Delta_g$, and $^2\Delta_u$ channels.[a]

Incident energy (Ry)	$^2\Sigma_g^+$	$^2\Sigma_u^+$	$^2\Pi_u$	$^2\Delta_g$	$^2\Delta_u$
0.05	27.73	0.55	0.44	0.01	
0.08	29.79	0.80	0.28	0.03	
0.10	30.89	0.98	0.17	0.06	
0.1102	31.18	1.07	0.13	0.08	0.0001
0.12	31.32	1.16	0.10	0.10	0.0002
0.13	31.37	1.26	0.09	0.13	0.0003
0.1396	31.37	1.38	0.09	0.15	0.0004
0.1543	31.30	1.54	0.11	0.19	0.0006
0.1764	31.14	1.83	0.20	0.26	0.0012
0.20	30.86	2.18	0.35	0.33	0.0020
0.22	30.51	2.46	0.53	0.40	0.0030
0.25	29.65	2.93	0.86	0.51	0.0050
0.30	27.42	3.72	1.57	0.71	0.0097
0.40	23.05	5.18	3.05	1.17	0.025

[a]In atomic units at $R=2.068$ a.u.

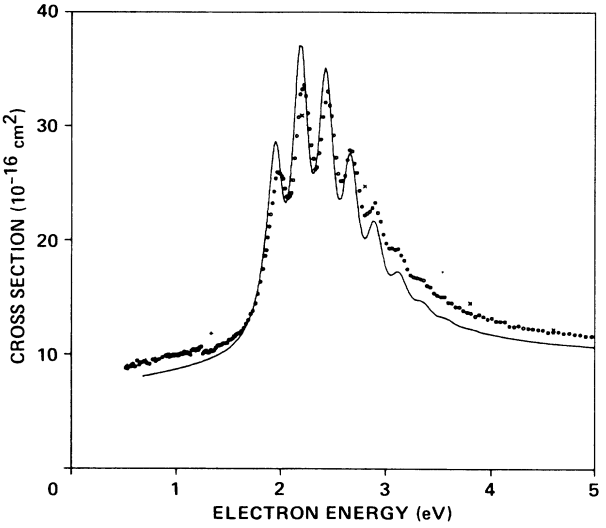

FIG. 1. Total electron scattering cross section for N_2. (——), present results; (○), experimental data of Kennerly, Ref. 22; (×), experimental data of Hoffman *et al.*, Ref. 23; (+), experimental data of Baldwin, Ref. 24.

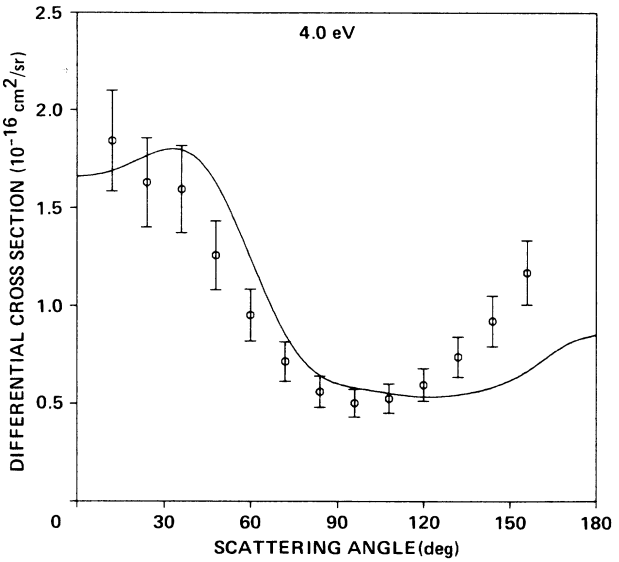

FIG. 3. e-N_2 elastic differential scattering cross section at 4.0 eV. (——), present results, and (○), experimental data of Shyn and Carignan, Ref. 25.

than experiment at the high-energy end.

The same hybrid treatment using a fixed-nuclei approximation and nuclear dynamics where appropriate was also used to determine electronically elastic differential cross sections. In this case we replace the $l=2$, $m=1$ fixed-nuclei partial-wave amplitude with the corresponding value from a vibrationally elastic nuclear dynamics calculation. Figures 2–8 compare the theoretical differential cross sections calculated at incident energies between 5.0 to 1.5 eV with the experimental measurements of Shyn and Carignan,[25] and Srivastava *et al.*[26] The incident energies can be separated into three regions. At 5.0, 4.0, and 3.0 eV (Figs. 2–4), the incident energy is above the $^2\Pi_g$ resonance. Theory reproduces the shape of the experimental curves rather well except that the experimental curves show stronger backscattering than our calculations. Also, at 4.0 and 5.0 eV, we find a small dip in the forward scattering. This feature is absent in the measurement at 4.0 eV, and the 5.0-eV data show a slight forward dip, but significantly weaker than theory. The calculations at 2.4, 2.1, and 1.9 eV (Figs. 5–7) typify the resonance region. The typical double minimum of the π_g partial wave is readily discernible in both theory and experiment. The largest devia-

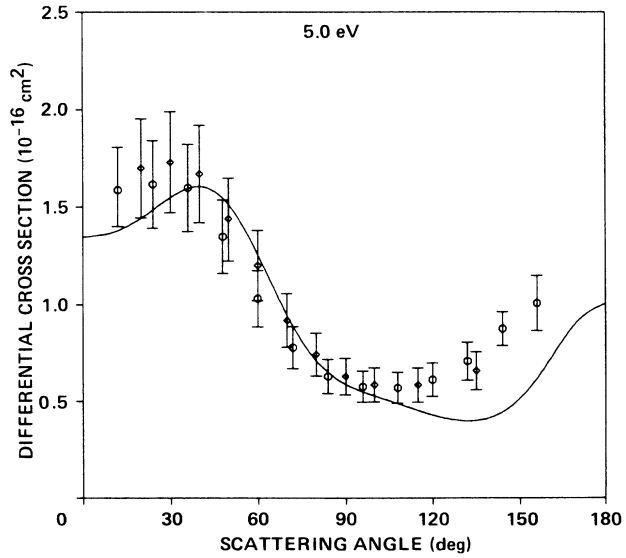

FIG. 2. e-N_2 elastic differential scattering cross section at 5.0 eV. (——), present results, (○), experimental data of Shyn and Carignan, Ref. 25, and (◇), experimental data of Srivastava *et al.*, Ref. 26.

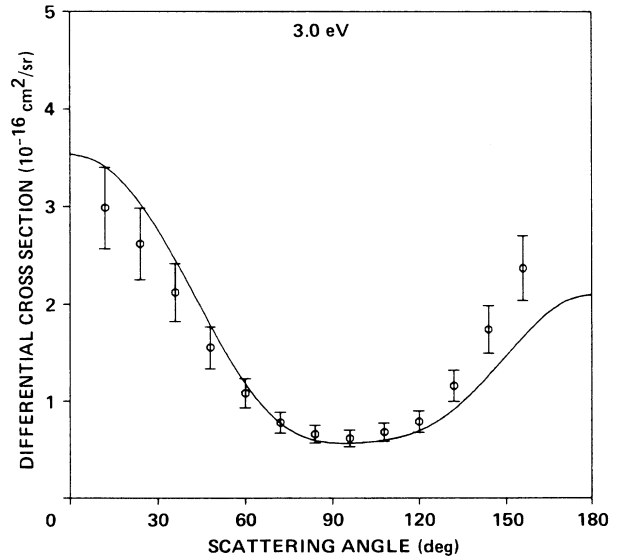

FIG. 4. e-N_2 elastic differential scattering cross section at 3.0 eV. (——), present results, and (○), experimental data of Shyn and Carignan, Ref. 25.

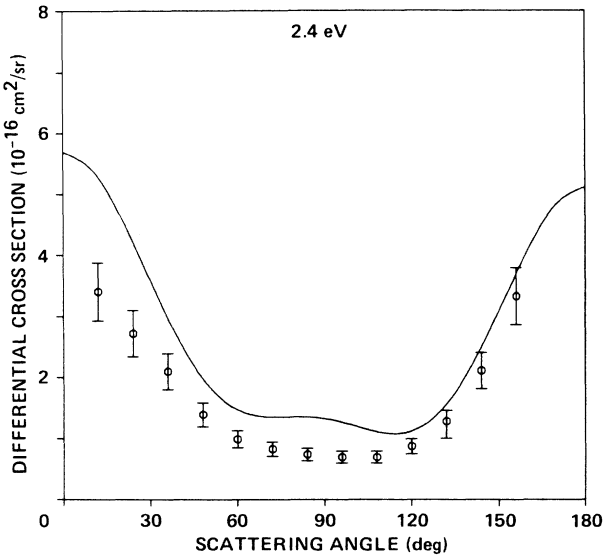

FIG. 5. e-N_2 elastic differential scattering cross section at 2.4 eV. (——), present results, and (○), experimental data of Shyn and Carignan, Ref. 25.

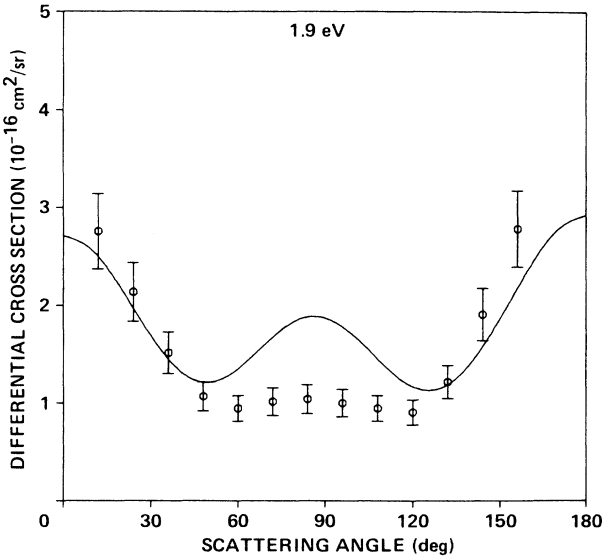

FIG. 7. e-N_2 elastic differential scattering cross section at 1.9 eV. (——), present results, and (○), experimental data of Shyn and Carignan, Ref. 25.

tion between theory and experiment is in the region between the two minima, with the theoretical curve rising more sharply than experiment. At 1.5 eV (Fig. 8) the calculated and experimental results are somewhat different, particularly in the forward and backward directions. Note, however, in the experimentally most accessible region between 30° and 120°, the agreement is satisfactory.[28]

ACKNOWLEDGMENTS

The research of W.M.H. is supported by NASA–Ames Cooperative Agreements No. NCC 2-147. The research at the California Institute of Technology is supported by NASA–Ames Cooperative Agreements No. NCC 2-319, the National Science Foundation, Grant No. PHY-8604242, and by the Innovative Science and Technology Program of the Strategic Defense Initiative Organization under Contract No. DAAL03-86-K-0140. One of us (M.A.P.L.) acknowledges the financial support from the Fundação de Amparo á Pesquisa do Estado de São Paulo (FAPESP), São Paulo, Brazil.

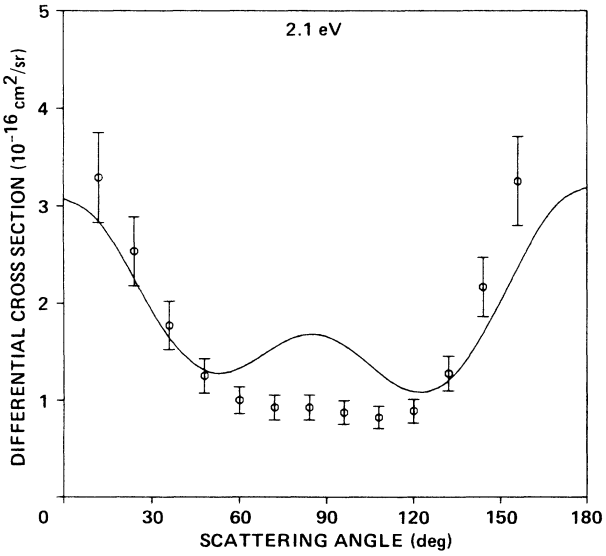

FIG. 6. e-N_2 elastic differential scattering cross section at 2.1 eV. (——), present results, and (○), experimental data of Shyn and Carignan, Ref. 25.

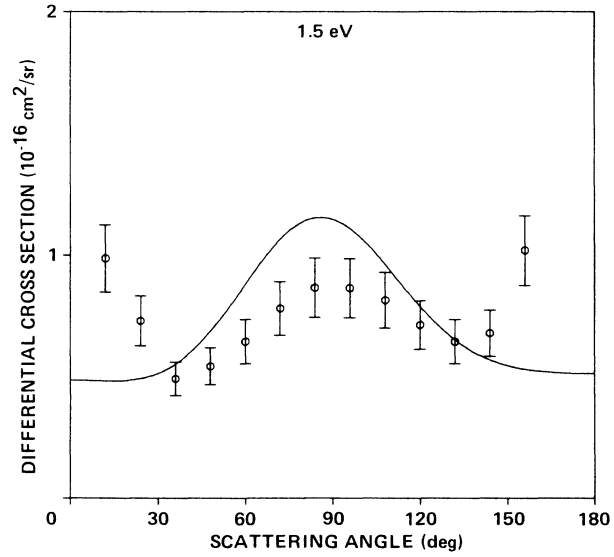

FIG. 8. e-N_2 elastic differential scattering cross section at 1.5 eV. (——), present results, and (○), experimental data of Shyn and Carignan, Ref. 25.

*Mailing address: NASA Ames Research Center, Mail Stop 230-3, Moffett Field, CA 94035.
†Present address: Instituto de Estudos Avançados, 12200 São José dos Campos, São Paulo, Brazil.
‡Present address: Department of Physics, Texas Tech University, Lubbock, TX 79409.

[1]N. F. Lane, Rev. Mod. Phys. **52**, 29 (1980).
[2]K. Onda and A. Temkin, Phys. Rev. A **28**, 621 (1983).
[3]T. L. Gibson and M. A. Morrison, Phys. Rev. A **29**, 2497 (1984).
[4]A. Temkin, Phys. Rev. **107**, 1004 (1957); A. Temkin and J. C. Lamkin *ibid.* **121**, 788 (1961).
[5]N. T. Padial and D. W. Norcross, Phys. Rev. A **29**, 1742 (1984).
[6]L. Castillejo, I. C. Percival, and M. J. Seaton, Proc. R. Soc. London, Ser. A **254**, 259 (1960).
[7]P. G. Burke, C. J. Noble, and S. Salvini, J. Phys. B **16**, L113 (1983).
[8]K. Takatsuka and V. McKoy, Phys. Rev. A **24**, 1267 (1981).
[9]K. Takatsuka and V. McKoy, Phys. Rev. A **30**, 2473 (1984).
[10]T. L. Gibson, M. A. P. Lima, K. Takatsuka, and V. McKoy, Phys. Rev. A **30**, 3005 (1984).
[11]W. M. Huo, T. L. Gibson, M. A. P. Lima, and V. McKoy, preceding paper, Phys. Rev. A **36**, 1632 (1987).
[12]A. Klonover and U. Kaldor, J. Phys. B **11**, 1623 (1978).
[13]B. I. Schneider and L. A. Collins, J. Phys. B **15**, L335 (1982).
[14]B. I. Schneider and L. A. Collins, Phys. Rev. A **27**, 2847 (1983).
[15]B. I. Schneider and L. A. Collins, Phys. Rev. A **30**, 95 (1984).
[16]M. Berman and W. Domcke, Phys. Rev. A **29**, 2485 (1984).
[17]W. M. Huo, T. L. Gibson, M. A. P. Lima, and V. McKoy (unpublished).
[18]P. J. Hay and T. H. Dunning, Jr., J. Chem. Phys. **64**, 5077 (1976).
[19]M. A. Morrison and L. A. Collins, Phys. Rev. A **17**, 918 (1978).
[20]T. L. Gibson, B. C. Saha, and M. A. Morrison, Phys. Rev. A (to be published).
[21]W. M. Huo, V. McKoy, M. A. P. Lima, and T. L. Gibson, in *Thermophysical Aspects of Re-Entry Flows,* Vol. 103 of *Progress in Astronautics and Aeronautics,* edited by J. N. Moss and C. D. Scott (American Institute of Aeronautics and Astronautics, New York, 1986), p. 152.
[22]R. E. Kennerly, Phys. Rev. A **21**, 1876 (1980).
[23]K. R. Hoffman, M. S. Dabaneh, Y.-F. Hsieh, W. E. Kauppila, V. Pol, J. H. Smart, and T. S. Stein, Phys. Rev. A **25**, 1393 (1982).
[24]G. C. Baldwin, Phys. Rev. A **9**, 1225 (1974).
[25]T. W. Shyn and G. R. Carignan, Phys. Rev. A **22**, 923 (1980).
[26]S. K. Srivastava, A. Chutjian, and S. Trajmar, J. Chem. Phys. **64**, 1340 (1976).
[27]S. Yagi (private communication).